

The Advantages of an Attenuated Total Internal Reflection Infrared Microspectroscopic Imaging Approach for Kidney Biopsy Analysis

HEATHER J. GULLEY-STAHL, SHARON B. BLEDSOE, ANDREW P. EVAN,
and ANDRÉ J. SOMMER*

Molecular Microspectroscopy Laboratory, Department of Chemistry and Biochemistry, Miami University, Oxford, Ohio 45056 (H.J.G.-S., A.J.S.); and Department of Anatomy and Cell Biology, Indiana University School of Medicine, Indianapolis, Indiana 46202 (S.B.B., A.P.E.)

The benefits of an attenuated total reflection Fourier transform infrared (ATR-FTIR) imaging approach for kidney biopsy analysis are described. Biopsy sections collected from kidney-stone formers are analyzed at the initial stages of stone development to provide insights into stone growth and formation. The majority of tissue analysis currently conducted with IR microspectroscopy is performed with a transfection method. The research presented in this manuscript demonstrates that ATR overcomes many of the disadvantages of transfection or transmission measurements for tissue analysis including an elimination of spectral artifacts. When kidney biopsies with small mineral inclusions are analyzed with a transfection approach, specular reflection and the Christiansen effect (anomalous dispersion) can occur, leading to spectral artifacts. Another effect specific to the analysis of mineral inclusions present in kidney biopsies is known as the *reststrahlen* effect whereby the inclusions become strong reflectors near an absorption band. ATR eliminates these effects by immersing the sample in a high index medium. Additionally, the focused beam size for ATR is decreased by a factor of four when a germanium internal reflection element is used, allowing the acquisition of spectra from small mineral inclusions several micrometers in diameter. If quantitative analysis of small mineral inclusions is ultimately desired, ATR provides the photometrically accurate spectra necessary for quantification.

Index Headings: ATR-FTIR imaging; Attenuated total reflection; Fourier transform infrared imaging; Transfection spectroscopy; Tissue analysis; Kidney biopsy; Kidney stone disease.

INTRODUCTION

The chemistry associated with kidney stone formation and growth is not well understood and has been the focus of many studies for the past seventy years. Fully formed urinary stones can be studied much like a geologist studies sedimentary rock to elucidate the chemistry during the growth of a stone. However, to study the cause for initial kidney stone formation, small mineral inclusions in tissue biopsies must be analyzed.^{1–3} For years, this type of analysis has relied on histological preparations, which involve producing thin sections followed by preferential staining. The stained tissue is then examined with an optical microscope. There are several limitations associated with histopathology, including the fact that the staining procedure involves multiple steps during which the material of interest may be lost or destroyed. In addition, this type of analysis relies on trained visual observation; therefore, the rate of misdiagnosis can be as high as ~30%.⁴ Infrared imaging methods can be employed to gain similar information as histopathology, but it is beneficial in that it also provides the

molecular information required for objective disease detection.^{5,6}

In 1996, Estepa-Maurice et al. described a method for the analysis of crystal deposits in kidney tissue biopsies using Fourier transform infrared (FT-IR) microscopy.⁷ Their investigation included two different sample preparations for transmission FT-IR microscopy analysis. The first sampling method required placing kidney biopsies with mineral inclusions directly on a CaF₂ window. Because CaF₂ windows are expensive and pathologists typically do not have them readily available, a second approach was investigated. This latter approach involved excising individual inclusions with a fine pointed probe and transferring them to a NaCl window for subsequent analysis. However, analyzing the mineral inclusions *ex situ* does not allow the investigator to gain a full understanding of the inclusion in its native environment. In addition, this type of analysis only permits particles in the range of 5–10 μm to be routinely studied.

In 2005, Anderson et al. developed a protocol utilizing IR microspectroscopy with a transfection approach to study mineral inclusions in tissue biopsies.⁸ Unlike the previous studies of Estepa-Maurice et al., this protocol allowed direct analysis of the biopsy with the use of a low-E glass slide. A low-E slide is a glass slide with a thin reflective coating that reflects nearly all mid-infrared radiation and is transparent to visible light. Therefore, the low-E glass slide permits both visual and IR images to be collected from the same sample. The transfection sampling method provides direct molecular identification of the species being studied on sample areas as small as 12 μm using a probe wavelength of 3 μm. Anderson et al. showed that within an IR image of a biopsy, many spectra will show a mixture of two or more components (e.g., tissue and hydroxylapatite). With the prevalence of kidney stone disease progressing specifically in industrialized countries, there is a need to obtain quantitative information from small mineral inclusions. This quantitative information may allow a better understanding of stone chemistry at the very initial stages of formation. However, spectral artifacts typically present in transfection spectra of tissues not only make sample identification difficult, but also do not provide the photometrically accurate spectra necessary for quantitative purposes.

Combining the disparate disciplines of histology and infrared microspectroscopy has proven to be beneficial for many biological applications. Many groups have used FT-IR microspectroscopic imaging for biomedical applications. Recently, Mendelsohn, Diem, and Bhargava have used infrared microscopy for the analysis of tissues for various applications including wound healing, cell analysis, and cancer diagnosis. These studies have typically relied on a transfection or

Received 22 May 2009; accepted 29 October 2009.

* Author to whom correspondence should be sent. E-mail: sommeraj@muohio.edu.

transmission sampling method for analysis.^{9–11} Recently, efforts to incorporate infrared microanalysis into a protocol for disease detection have settled on the use of reflective substrates, most commonly low-E glass slides, in conjunction with transflection spectroscopy. Although this approach is a useful method for tissue analysis, it can pose several limitations. Transflection is typically a straightforward analysis, provided the sample is a continuous film with low contrast interfaces. Low contrast interfaces are characterized as those having optically similar materials present on either side of the interface where the refractive index of both materials becomes the most important parameter. However, many tissue sections do not meet these criteria and contain discontinuities such as blood vessels and in the current case, mineral inclusions, which can present high contrast edges, promoting scattering, diffraction, reflection, and dispersion. All of these optical effects can manifest in the spectrum in a variety of ways. Further, these effects are amplified due to the size and shape of the sample and the high convergence of the impinging infrared radiation. In the current case, in which small mineral inclusions are surrounded with tissue, not only does the mineral present a high contrast edge, but it also acts as a highly scattering point defect. This phenomenon is known as the Christiansen effect, whereby the sample exhibits anomalous dispersion near an absorption band. Mineral inclusions can also exhibit the reststrahlen effect, whereby the sample becomes a strong reflector near an absorption band.^{12,13} Reststrahlen bands are usually associated with the reflection that occurs at the strongest bands of ionic materials and metals, but it has been shown that this effect is not limited to these substances.¹⁴ When collecting infrared spectra from a kidney biopsy with transflection spectroscopy, any or all of these effects can occur simultaneously. Therefore, it is difficult to determine which effect dominates over another, especially when the spectra usually possess several distortions from a combination of effects. From a quantitative perspective, the adherence of the Beer–Lambert law dictates that the sole mechanism for the attenuation of light must be absorption and the optical path length through the sample must be well known. With transflection and transmission approaches, scattering and diffraction will prominently affect the former and changes in refractive index will affect the latter.

In 1991, Sommer reported on dispersive band shapes in IR microspectroscopy and later Stewart and Sommer demonstrated that these optical nonlinearities increase with a greater difference in refractive index between the two materials. Further, the magnitude of the effect increases with a decreasing spatial domain of one material embedded in the other.^{15–17} Consider the simple case of an air/tissue interface within a tissue biopsy. The difference in refractive index between these two materials is ~ 0.40 . When an IR spectrum is obtained at such an interface, portions of the light will undergo specular (Fresnel) reflection and anomalous dispersion, which are manifested in the spectrum as derivative-shaped peaks. Later, in 1998, Bhargava demonstrated that spectral artifacts are observed when imaging the interface of polymer-dispersed liquid crystals.¹⁸ Bhargava described the optical effects that occur when imaging multicomponent systems and how these effects can complicate quantitative analyses. More recently, in 2005, Romeo and Mohlenhoff reported the observation of dispersive line shapes from scattering and/or diffraction when analyzing tissue samples with a transflection or diffuse

reflection approach.^{19–21} Romeo proposed a computational method to reduce the dispersive artifact that causes an abnormal ratio of the amide I and II bands, a lower wavenumber shift of bands, and a sloping baseline. Their approach is very similar to the conversion of a Fresnel reflection spectrum to the optical constant (n and k) spectra using Fourier transform. The authors explained that these spectral artifacts make correct identification of disease states difficult and have a significant influence on statistical analyses, but they also state that their computational correction is not completely ideal. In 2005, Mohlenhoff stated that these artifacts need to be firmly understood before IR microspectroscopy can be utilized as a diagnostic indicator of disease.

A method that overcomes these limitations is attenuated total internal reflection (ATR) infrared microspectroscopy.²² ATR with a germanium internal reflection element (IRE) can eliminate all of the previously mentioned spectral artifacts.^{8,22,23} However, Bhargava has shown that other IRE types such as diamond do not eliminate all spectral artifacts due to the increased penetration depth.¹⁴ ATR also provides a decreased focus beam size by immersing the sample in a high index medium, similar to immersion microscopy.²⁴ Unlike immersion microscopy, which employs a high index liquid, ATR infrared microspectroscopy employs a solid germanium hemisphere commonly known as an IRE. The IRE is placed into intimate contact with the sample and infrared light is internally reflected, producing an evanescent wave that probes the sample to a depth of 0.063λ (assuming the angle of incidence is 45° and the refractive index of the sample is 1.5). The diffraction-limited diameter for light focused to a point is defined as the bright central maximum of the Airy disk and is given by:

$$d = \frac{1.22\lambda}{NA} \quad (1)$$

$$NA = n_1 \sin \theta \quad (2)$$

where λ is the wavelength of light employed and NA is the numerical aperture of the system. The NA is defined as the product of the refractive index of the medium in which the sample is immersed (n_1) and $\sin \theta$, where θ is the half angle acceptance of the optic. This equation is only valid for a circular aperture that is uniformly filled.²⁵ Because transflection typically uses half the objective to excite the sample and the other half to collect the reflected light, the aperture is no longer circular. Although the half angle acceptance does not change, the above equation may not give a good estimate of the diffraction-limited diameter for a reflection measurement. However, for the current system and those investigated by Tisinger, the focused beam diameter measured in reflection is twice that of the focused beam diameter measured in transmission (essentially reducing the numerical aperture by a factor of two).²⁶ No matter what perspective is taken, the focused beam diameter in transflection ($n_1 = 1.0$) will be four times larger than that for ATR when using a germanium hemisphere ($n_1 = 4.0$). The diffraction-limited spot size at the microscope focus is reduced by the refractive index of the IRE, thereby increasing the spatial resolution. In addition to increasing the spatial resolution of the measurement, ATR microspectroscopy eliminates significant sample preparation associated with transmission measurements and spectral



FIG. 1. ATR imaging accessory.

artifacts associated with transmission and transfection measurements.

The development of ATR occurred over forty years ago when Harrick and Fahrenfort employed the method to study the infrared spectra of organic materials.^{27,28} Currently, there are two approaches for ATR imaging: on- and off-axis imaging. With on-axis ATR imaging, the hemisphere/sample composite is centered at the microscope's focus and illuminated globally. Radiation that is internally reflected is then imaged onto a two-dimensional array detector. On the other hand, off-axis ATR imaging requires the hemisphere/sample composite to be initially centered at the microscope's focus and then imaging is conducted by moving the composite off-axis. The development and commercialization of off-axis ATR imaging has taken place over the last 15 years. In 1992 and 1994, Nakano and Kawata performed off-axis ATR measurements and reported an improvement in spatial resolution equal to the refractive index of the germanium IRE.^{29,30} Although Nakano and Kawata were the first to report this improvement for ATR, the concept of immersion has long been known and employed by optical designers to collect and focus more available light onto a small area detector. The size of the detector could be reduced by a factor equal to the refractive index if the detector was placed in optical contact with the plano surface of the hemisphere.³¹ Later, Lewis and Sommer reported on the approach taken by Nakano et al., but on a commercial PerkinElmer i-series microscope.^{32,33} The next significant development of off-axis ATR imaging came in 2006, when Patterson and Havrilla employed a 12.5 mm diameter hemisphere and demonstrated that spherical aberrations limiting the total sampled area were directly related to the radius of the hemisphere.³⁴ Later in 2006, PerkinElmer developed and introduced an ATR accessory based on the work of the off-axis imaging concept of Nakano et al. and Lewis et al.³⁵

The goal of this study is to demonstrate the capabilities and benefits of an off-axis ATR imaging approach over existing methodologies, principally transfection spectroscopy, for examining small mineral inclusions within kidney tissue. The future goal is to extend this type of analysis to allow quantitative analysis of small mineral inclusions that may be of mixed composition at the localized mineral/tissue interface.³⁶

EXPERIMENTAL

Kidney biopsies were obtained from Indiana University Medical School and were prepared by a histologist. Biopsies

were thinly sliced ($\sim 5 \mu\text{m}$ thick) and mounted on low-E glass slides (Kevley Technologies, Chesterland, OH) for ATR imaging analysis. A serial section stained with Yasue silver replacement was employed as a control section. Prior to infrared analysis, the control was visibly examined with an Olympus white light microscope (20 \times objective) to determine the areas of interest. Biopsies employed for ATR-FTIR imaging were not stained.

Samples were analyzed with a PerkinElmer Spectrum Spotlight 300 infrared imaging microscope equipped with a liquid nitrogen cooled HgCdTe (MCT) 16×1 linear array detector for the rapid acquisition of molecular images; this detector has a cut-off of 720 cm^{-1} . Instrumentation optics allow a 1:1 or 4:1 imaging of the area on the detector elements, resulting in 25×25 or $6.25 \times 6.25 \mu\text{m}$ pixel resolution in the transmission or reflection mode. The ATR imaging accessory displayed in Fig. 1 employs a germanium hemisphere having a refractive index (n_c) of 4.0. As a result, the pixel resolution is increased by a factor of four (n_c) to $1.56 \mu\text{m}$. This accessory easily fits into the motorized stage of the infrared microscope. Next, the sample is loaded onto a small stage that is manually maneuvered to locate areas of interest. Finally, the arm containing the IRE swings over the sample and lowers down onto the sample for data collection. Due to spherical aberrations associated with large off-axis positions, the image collected by the ATR accessory is limited to an area of $\sim 400 \times 400 \mu\text{m}$. For the IR images presented in this investigation, spectra were collected at 16 cm^{-1} resolution and 32 scans were averaged per pixel. For point-mode collection, the system employed a $100 \times 100 \mu\text{m}$ liquid nitrogen cooled MCT detector. A $100 \mu\text{m}$ germanium drop-down ATR accessory and a $50 \times 50 \mu\text{m}$ aperture were employed for single-point measurements. The point-mode spectra represent the average of 64 individual scans possessing a spectral resolution of 4 cm^{-1} .

RESULTS AND DISCUSSION

In 2005, Romeo et al. proposed a computational method for the reduction of dispersive line shapes observed when utilizing diffuse reflection or transfection infrared microspectroscopy.¹⁹ Despite the effectiveness of their computational correction, such a modification should only be utilized when all experimental options have been exhausted. A solution to the problem has been in practice since well before the advent of infrared microspectroscopy and involves embedding the sample in a matrix of similar refractive index.³⁷ Traditionally, this approach is commonly achieved with infrared spectroscopy by preparing Nujol mulls. An experimental technique relying on the same principles as Nujol mulls involves the placement of Nujol and a 1 mm thick barium fluoride (BaF_2) coverslip over a biopsy sample prior to infrared analysis to reduce dispersive line shapes.

To demonstrate the application of this technique to scattering samples, a kidney biopsy mounted on a low-E glass slide was analyzed with transfection spectroscopy. Spectra collected around the perimeter of the tissue section and at the edges of vesicles within the biopsy produce dispersive artifacts shown in Fig. 2a. Figure 2a demonstrates two artifacts commonly observed with a transfection approach, caused by dispersion and scattering. A monotonically sloping baseline occurs as a result of scattering and a sloping baseline localized near an absorption results from the Christiansen effect where imping-

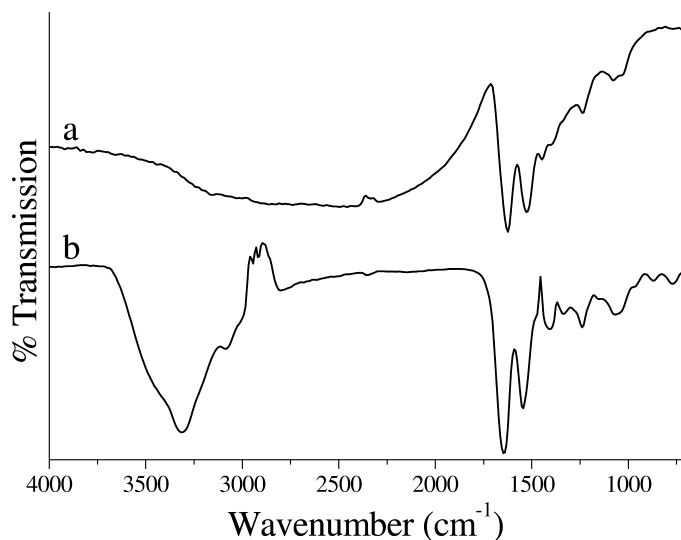


FIG. 2. Transfection analysis of a kidney biopsy mounted on a low-E glass slide. (a) Spectrum collected from tissue edge showing spectral artifacts (sloping baseline and derivative shape at $\sim 1700\text{ cm}^{-1}$). (b) Spectrum taken from same location as (a) after application of nujol and a BaF_2 window; sloping baseline and derivative shape are reduced.

ing radiation experiences anomalous dispersion at high contrast edges. The spectrum also contains a derivative shape on the leading edge of the amide I absorption at $\sim 1650\text{ cm}^{-1}$ due to specular reflection at the tissue/air interface. A spectrum from the same location is presented in Fig. 2b after the application of Nujol and a BaF_2 coverslip. As can be observed, the sloping baseline and derivative shape are both eliminated. The only artifacts remaining are uncompensated C–H stretching (2900 cm^{-1}) and bending (1450 cm^{-1}) absorption bands from the Nujol. This simple Nujol/ BaF_2 coverslip sampling method eliminates the need for computational methods; however, the C–H stretching and bending regions of the spectrum will be dominated by the Nujol absorption. A similar approach for improving spectral artifacts when analyzing tissue with a transfection approach is to leave the embedding medium in the sectioned tissue. During histological preparation, paraffin is absorbed into all parts of the tissue to aid in storing and sectioning the biopsy. The paraffin is then removed and the tissue is rehydrated for staining. Because the stain is not required for IR analysis, analyzing the tissue enveloped with paraffin should also produce similar results to the Nujol/ BaF_2 approach.

Although the Nujol/ BaF_2 window method of analysis does reduce the artifacts commonly observed with transfection spectroscopy, it is not completely ideal. When considering the interaction of infrared light with a kidney biopsy using a transfection approach, there are several optical effects that can give rise to spectral artifacts and these effects need to be carefully considered in order to properly interpret the data. Figure 3 presents a schematic demonstrating the various paths infrared light can take when interacting with a kidney biopsy. Ray “a” shows that light can experience Fresnel, or specular, reflection at high contrast edges (tissue/air interface), leading to derivative-shaped bands in the spectrum.^{16,26} Scattering can also occur at high contrast edges (mineral inclusion/tissue interface) as demonstrated by ray “b” leading to a sloping baseline in the spectrum. Scattering can be classified as large or small (Rayleigh) particle scattering. Rayleigh scattering occurs

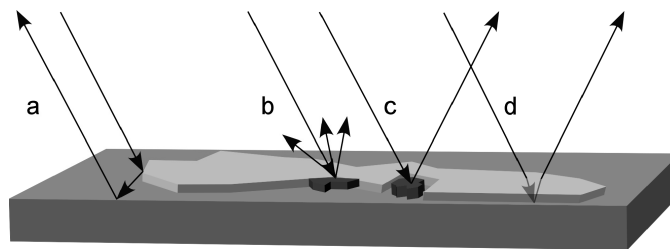


FIG. 3. Schematic demonstrating the various optical effects that can occur when infrared light impinges on a kidney biopsy. High contrast edges can promote (a) specular reflection, (b) scattering and (c) the mineral inclusion can exhibit the reststrahlen effect. Ray (d) demonstrates the normal process of transfection as the infrared beam is passed through the sample twice before reaching the detector.

for particles with dimensions 5–10% of the incident wavelength, whereas large-particle scattering occurs for particles with dimensions greater than 10% of λ .³⁸ Considering the various sized features present in a tissue biopsy with mineral inclusions, the scattering could result from both Rayleigh and large-particle scattering. In the case of ray “c”, the mineral inclusion surrounded by tissue can become a strong reflector near a strong absorption band, causing reststrahlen bands (peak inversion) to appear in the spectrum. Reststrahlen bands are specific for inorganic minerals and are only observed when analyzing the mineral portion of the kidney biopsy. When analyzing kidney biopsies it is expected that a combination of effects will occur and it is difficult to determine which effect will dominate over another unless prior information about the sample is known. Ray “d” demonstrates the normal process of transfection as the infrared beam is passed through the sample twice before reaching the detector.

If photometrically accurate spectra are desired with a transfection analysis, the thickness of the sample should be half that used for transmission ($\sim 3\text{ }\mu\text{m}$) due to the extended ($2\times$) optical path length (OPL). Otherwise, the strongly absorbing amide I and II bands may become totally absorbing. It is also important to note that all the artifacts previously discussed are path length dependent. Therefore, by reducing the OPL, the effects can be minimized. For example, when collecting a transmission measurement on a sample that is $6.0\text{ }\mu\text{m}$ thick with an average incidence angle of 27° , the OPL through the sample ($n_{\text{tissue}} = 1.4$) is $9.4\text{ }\mu\text{m}$, but with transfection the OPL doubles to approximately $18.8\text{ }\mu\text{m}$ because the light effectively passes through the sample two times. Alternatively, with an ATR approach, the optical path length through the sample will depend on penetration depth. With a Ge IRE, the penetration depth can be reduced to less than $1\text{ }\mu\text{m}$. However, because other IRE materials such as diamond will experience a larger penetration depth, some spectral artifacts may still be observed, but to a lesser degree.¹⁴

The bottom spectrum in Fig. 4 demonstrates two of the previously mentioned spectral artifacts as a calcium oxalate monohydrate (COM) mineral inclusion was analyzed with transfection point-mode collection utilizing a $50 \times 50\text{ }\mu\text{m}$ aperture. Because of scattering, a sloping baseline from short to long wavelengths is evident and derivative-shaped bands are located around 1750 and 800 cm^{-1} due to the effect of anomalous dispersion. All of these spectral artifacts and totally absorbing bands make proper identification of this mineral inclusion difficult. It is also important to note that the spectrum

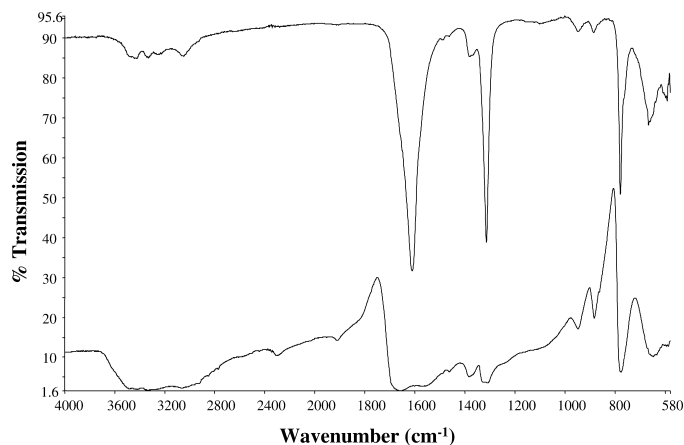


FIG. 4. (**Bottom**) Spectrum collected from a COM mineral inclusion with transflection spectroscopy, demonstrating various spectral artifacts such as a sloping baseline and derivative-shaped bands at 1750 cm^{-1} and 810 cm^{-1} . (**Top**) The ATR spectrum collected from the same location, showing a reduction in spectral artifacts.

also exhibits features from surrounding tissue with amide I and II bands evident at 1650 and 1540 cm^{-1} .

The top spectrum in Fig. 4 is a spectrum collected from the same location, but with a drop-down $100\text{ }\mu\text{m}$ ATR accessory also utilizing a $50 \times 50\text{ }\mu\text{m}$ aperture (sampled area is $12.5 \times 12.5\text{ }\mu\text{m}$). Due to the decreased beam diameter at the microscope focus for ATR, the upper spectrum in Fig. 4 does not possess any features of tissue, verifying that the ATR spectrum is purely from COM. The spectrum also demonstrates the ability of ATR to eliminate all spectral artifacts, allowing straightforward identification of the mineral inclusion as COM. Characteristic absorptions include the antisymmetric carboxylate C–O stretch at 1620 cm^{-1} , the 1315 cm^{-1} symmetric carboxylate C–O stretch, and the C–O bend at 780 cm^{-1} . The y-axis of Fig. 4 shows that the ATR spectrum (upper) represents a photometrically accurate infrared spectrum in which the percent transmission ranges from 96 to 33 percent and the baseline is relatively flat. On the other hand, the transflection spectrum (bottom) exhibits a percent transmission range of 30 to 2 percent. Therefore, in addition to allowing straightforward identification of the inclusion the method, as demonstrated by the upper spectrum in Fig. 4, could also allow an uncomplicated quantitative analysis due to its photometric accuracy.

Another example of a highly contaminated spectrum and the corresponding ATR spectrum is shown in Fig. 5. The lower spectrum in Fig. 5 was collected with a $50 \times 50\text{ }\mu\text{m}$ aperture using transflection spectroscopy. Although this spectrum demonstrates an extreme case of spectral distortions, the artifacts present are commonly observed in this laboratory. Figure 5, bottom, exhibits a non-zero or sloping baseline and inverted bands at 1140 and 625 cm^{-1} . The inverted bands are a result of the reststrahlen effect, whereby the hydroxylapatite mineral is becoming a strong reflector at those absorptions bands. The reststrahlen bands are also shifted to a higher frequency or shorter wavelength in the spectrum. The dashed lines in the spectrum were added to allow easier visualization of this wavelength shift. All of these spectral artifacts make identification of this mineral inclusion difficult. The ATR spectrum collected with the drop-down ATR accessory also utilizing a $50 \times 50\text{ }\mu\text{m}$ aperture is displayed as the top spectrum

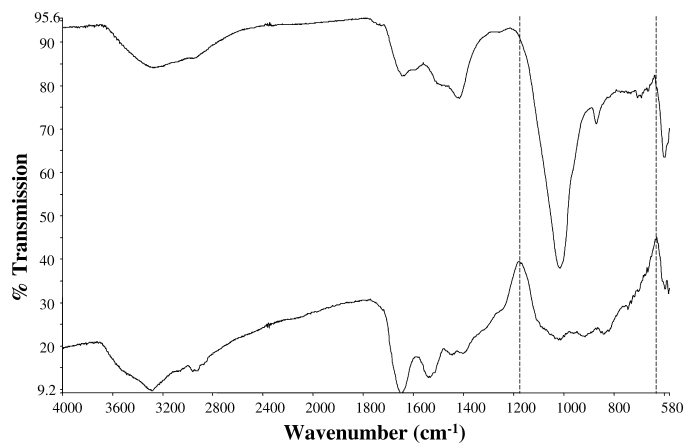


FIG. 5. (**Bottom**) Spectrum collected from a HAP mineral inclusion with transflection spectroscopy, demonstrating spectral artifacts such as a sloping baseline and reststrahlen bands at 1140 and 625 cm^{-1} . The reststrahlen bands are also shifted to a higher frequency. (**Top**) The ATR spectrum collected from the same location, showing a reduction in spectral artifacts.

in Fig. 5. The ATR spectrum shows a reduction in spectral artifacts and the strong phosphate absorption at 1010 cm^{-1} allows straightforward identification of this mineral as hydroxylapatite.

A comparative study of ATR and transflection imaging was investigated for kidney biopsy analysis to determine the benefits and disadvantages of each. Figure 6a shows the visible image of a stained tissue section with $\sim 20\text{--}30\text{ }\mu\text{m}$ COM mineral inclusions in the papilla of the kidney. Transflection analysis was completed on the same area of a serial unstained section and is displayed in Fig. 6b. A $400 \times 400\text{ }\mu\text{m}$ area was imaged with a $6.25\text{ }\mu\text{m}$ pixel resolution. Principal component analysis was conducted on the image to determine the number of unique chemical components present in the field of view. The yellow/green areas indicate mineral inclusions, the red areas are tissue, and the blue areas are the low-E glass substrate. Each pixel in the image represents an infrared spectrum and the representative spectra shown in Fig. 7 are taken from various locations of the transflection image.

Figure 7a is the infrared spectrum collected from a mineral inclusion (yellow/green area). The spectrum contains several spectral artifacts including a sloping baseline from short to longer wavelengths and derivative shaped bands caused by scattering and the Christiansen effect. Figure 7a also contains contributions from tissue evident by the amide I and II bands present at 1650 and 1560 cm^{-1} . These tissue features demonstrate that transflection with a $6.25\text{ }\mu\text{m}$ pixel resolution was not able to isolate a spectrum from a $\sim 20\text{ }\mu\text{m}$ mineral inclusion. Figure 7b is a tissue spectrum taken from the transflection image, which contains spectral artifacts including a sloping baseline and a derivative shape on the leading edge of the amide I absorption. Despite easy identification of the material as tissue due to the presence of the amide I and II bands at 1650 and 1560 cm^{-1} , the spectral artifacts of this tissue spectrum could make quantitative analysis a challenge.

Figure 6c displays the ATR image collected from the same area as Fig. 6b. The image area was again $400 \times 400\text{ }\mu\text{m}$, but collected with a four-fold increase in pixel resolution to $1.56\text{ }\mu\text{m}$ due to the use of a germanium hemisphere ($n_c = 4.0$). Visual inspection of the ATR image shows improved clarity as the mineral inclusions are better defined from tissue, indicating

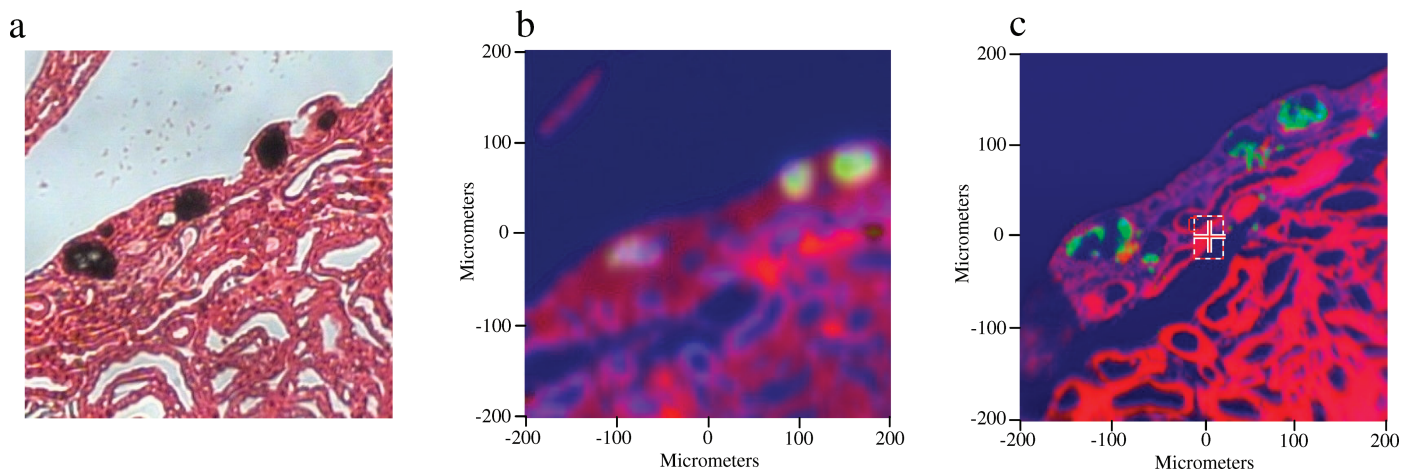


FIG. 6. (a) White light microscope visible image of a stained tissue section containing $\sim 20\text{--}30\ \mu\text{m}$ calcium oxalate monohydrate inclusions. (b) Transflection image of unstained serial tissue section comparable to area shown in (a). (c) ATR image of the same area observed in (b).

an increased spatial resolution. Representative spectra extracted from this image are shown in Fig. 8. Figure 8a is a spectrum from the COM inclusion (yellow area), demonstrating the elimination of spectral artifacts including the sloping baseline and derivative-shaped band observed in Fig. 7a. The flat baseline and well-defined bands allow straightforward identification of this mineral inclusion as COM. There are no contributions from tissue (amide bands), demonstrating that due to a decreased focused beam size, the ATR spectrum is purely from the COM inclusion. The spectrum of tissue taken from the ATR image is shown in Fig. 8b. Unlike the spectrum from Fig. 7b, the ATR spectrum baseline is not sloping from short to longer wavelengths and there are no derivative-shaped artifacts. From a photometric standpoint, the ATR spectra could lend themselves to a less problematic quantitative analysis.

Smaller hydroxylapatite (HAP) mineral inclusions in the papilla of the kidney on the order of $5\text{--}20\ \mu\text{m}$ were also analyzed with both transflection and ATR imaging. The visible image of the stained tissue section with HAP inclusions is shown in Fig. 9a. The transflection infrared image collected from a comparable area of an unstained serial tissue section is

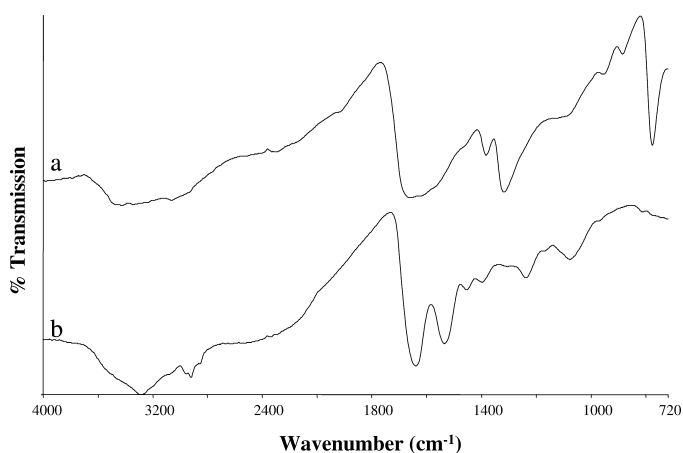


FIG. 7. IR spectra taken from the transflection image in Fig. 6b. (a) Spectrum collected from mineral inclusion, and (b) spectrum collected from tissue. Spectral artifacts (sloping baseline and derivative-shaped bands) are evident.

shown in Fig. 9b. The same principal component analysis was conducted on the image as previously described. Three chemically distinct areas are visible from the image, but many of the smaller mineral inclusions are not detected with the transflection approach as their size becomes smaller than the pixel resolution ($6.25\ \mu\text{m}$). Representative spectra from the transflection image are displayed in Fig. 10. Figure 10a is the spectrum from a mineral inclusion (yellow area) demonstrating several spectral artifacts. A sloping baseline, and the characteristic derivative shape of the bands at $1750\ \text{cm}^{-1}$ and $1250\ \text{cm}^{-1}$, makes proper spectral identification difficult. The tissue spectrum (Fig. 10b) possesses a similar sloping baseline from scattering as that shown and discussed in Fig. 7b.

An ATR image collected from the same area is presented in Fig. 9c. Due to the four-fold decrease in spot size, the ATR image in Fig. 9c distinctly shows several very small mineral inclusions not previously detected with transflection. The spectra collected from the ATR image are shown in Fig. 11. The ATR spectra are free of the spectral artifacts displayed in Fig. 10. The antisymmetric $\nu_3\ \text{PO}_4^{3-}$ band at $1010\ \text{cm}^{-1}$ in Fig. 11a allows straightforward identification of the mineral

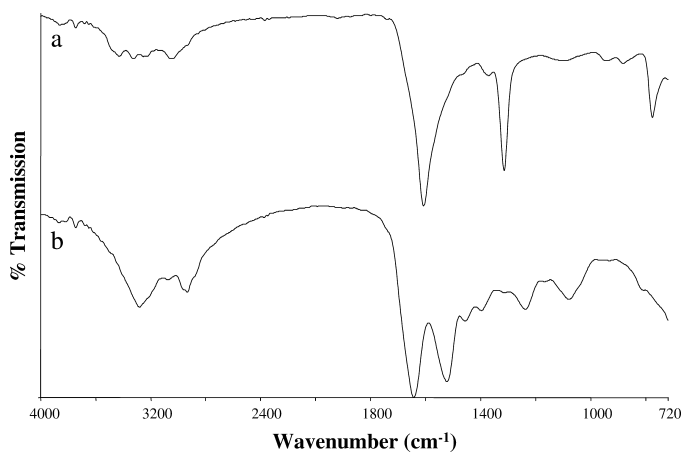


FIG. 8. IR spectra taken from the ATR image in Fig. 6c. (a) Spectrum collected from mineral inclusion, and (b) spectrum collected from tissue. Notice the elimination of the spectral artifacts (sloping baseline and derivative-shaped bands) observed in Fig. 7.

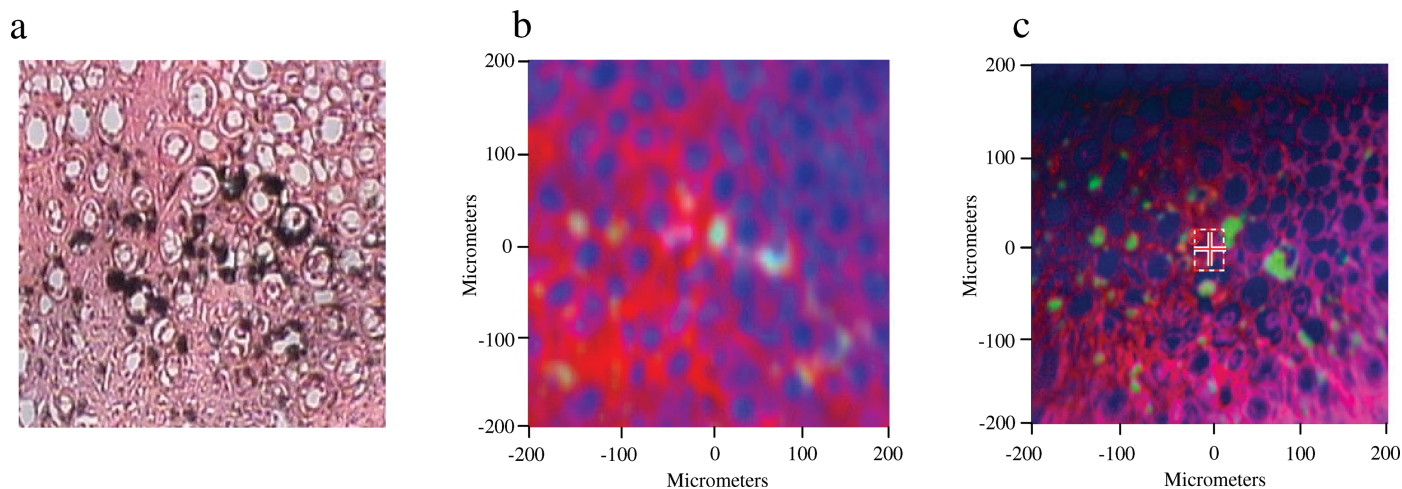


FIG. 9. (a) White light microscope visible image of a stained tissue section containing $\sim 5\text{--}20\ \mu\text{m}$ hydroxylapatite (HAP) mineral inclusions. (b) Transflection image of unstained serial tissue section comparable to area shown in (a). (c) ATR image of the same area observed in (b).

inclusion as HAP. Also, the tissue spectrum from the ATR image shown in Fig. 11b is free of spectral artifacts.

CONCLUSION

The results of this study demonstrate that ATR imaging of tissue sections can overcome many of the limitations associated with transmission and transflection analyses. In comparison to transmission analysis, ATR imaging eliminates spectral artifacts and, most importantly, the lengthy sample preparation methods associated with transmission. Although the sample preparation for ATR imaging is similar to that for transflection imaging, the ATR method eliminates spectral artifacts and provides an increased spatial resolution. With the use of a germanium IRE ($n_c = 4.0$), the focused beam size is decreased to 0.5λ , which is a fourfold improvement over transflection analysis when considering conventional instrumentation.^{24,35}

Two potential limitations of the ATR method are that the samples could be damaged after direct contact with the IRE and that the total image area is rather small compared to transmission and transflection. Considering the first limitation, in the current case of kidney biopsies and other cases (e.g.,

breast and prostate biopsies), there is always more than enough sample for multiple analyses. Assuming the limiting case of a 1 mm diameter biopsy that is 1 mm in length, a 6 μm thick tissue section taken from such a biopsy represents less than 1% of the total sample. Most kidney, breast, and prostate biopsies are significantly larger than this limiting case. Considering the second limitation, specifically for disease detection, successful cancer histopathology using 500 μm diameter circular sections has been demonstrated.⁹ This area is comparable to the $400 \times 400\ \mu\text{m}$ image areas collected using the current accessory. Furthermore, Patterson et al. demonstrated that a $2500 \times 2500\ \mu\text{m}$ image area can be obtained with the use of a larger 12.5 mm diameter IRE. With the use of this device, an $800 \times 800\ \mu\text{m}$ image area could be obtained without any sacrifice in spatial resolution.²⁶

To conclude, this research has shown that the ATR method provides four important advantages for biopsy analysis: (1) The method with the current sampling accessory is routine. (2) It provides a decreased focused beam size at the microscope's focus using conventional instrumentation without the use of computational approaches and/or synchrotron sources. (3) Many

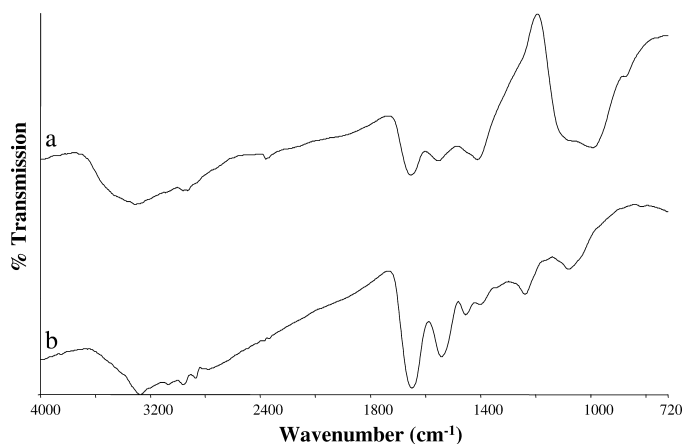


FIG. 10. IR spectra taken from the transflection image in Fig. 9a. (a) Spectrum collected from mineral inclusion, and (b) spectrum collected from tissue. Spectral artifacts (sloping baseline and derivative-shaped bands) are evident.

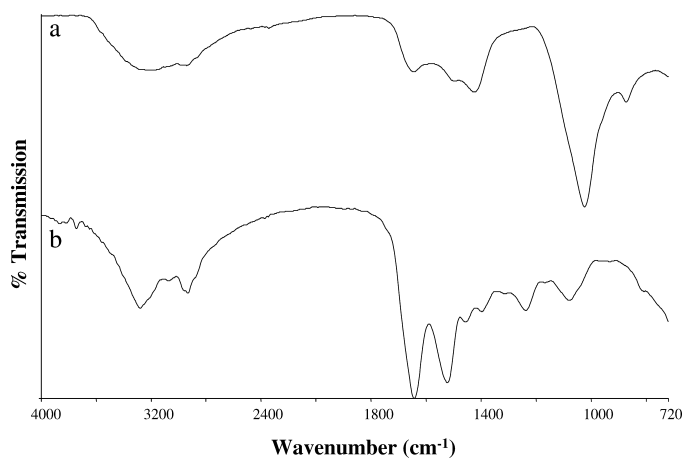


FIG. 11. IR spectra taken from the ATR image in Fig. 9c. (a) Spectrum collected from mineral inclusion, and (b) spectrum collected from tissue. Notice the elimination of the spectral artifacts (sloping baseline and derivative-shaped bands) observed in Fig. 10.

of the spectral artifacts associated with transmission and transfection analyses are eliminated. (4) Finally, it provides the best photometrically accurate spectra, required for proper disease detection. Future work includes utilizing the reported ATR images in conjunction with appropriate calibration curves for the quantitative analysis of mixed mineral inclusions.

ACKNOWLEDGMENTS

The authors would like to thank the editor Dr. Peter Griffiths for his helpful suggestions and useful discussions. We would also like to thank Kodak, Lexmark International, Perkin Elmer, and Procter & Gamble for financial support of this project.

1. R. L. Ryall, *Urol. Res.* **36**, 77 (2008).
2. A. P. Evan, F. L. Coe, J. E. Lingeman, Y. Shao, A. J. Sommer, S. B. Bledsoe, J. C. Anderson, and E. M. Worcester, *Anat. Rec.* **290**, 1315 (2007).
3. A. Evan, J. Lingeman, F. L. Coe, and E. Worcester, *Kidney Int.* **69**, 1313 (2006).
4. G. P. Kasidas, C. T. Samuella, and T. B. Weir, *Ann. Clin. Biochem.* **41**, 91 (2004).
5. R. Bhargava and I. W. Levin, *Spectrochemical Analysis Using Infrared Multichannel Detectors* (Blackwell Publishing, Oxford, England, 2005).
6. R. Bhargava and I. W. Levin, *Vib. Spectrosc. Med. Diagnosis*, 155 (2008).
7. L. Estepa-Maurice, C. Hennequin, C. Marfisi, C. Bader, B. Lacour, and M. Daudon, *Am. J. Clin. Pathol.* **105**, 576 (1996).
8. J. Anderson, J. Dellomo, A. Sommer, A. Evan, and S. Bledsoe, *Urol. Res.* **33**, 213 (2005).
9. R. Bhargava, *Anal. Bioanal. Chem.* **389**, 1155 (2007).
10. M. Diem, S. Boydston-White, and L. Chiriboga, *Appl. Spectrosc.* **53**, 148A (1999).
11. R. Mendelsohn, A. L. Boskey, and N. P. Camacho, "Infrared microscopy and imaging of hard and soft tissues", in *Spectrochemical Analysis Using Infrared Multichannel Detectors*, R. Bhargava and I. W. Levin, Eds. (Blackwell Publishing, Oxford, England, 2005), p. 234.
12. W. W. Wendlandt and H. G. Hecht, *Reflectance Spectroscopy* (John Wiley and Sons, New York, 1966).
13. G. Kortum, *Reflectance Spectroscopy* (Springer-Verlag, New York, 1969).
14. R. Bhargava, "Next Generation Infrared Imaging for Biomedical Spectroscopy", Presented at the 37th Annual Conference of the Federation of Analytical Chemistry and Spectroscopy Societies (Louisville, KY, October 2009).
15. A. J. Sommer and J. E. Katon, *Appl. Spectrosc.* **45**, 1633 (1991).
16. A. J. Sommer, "Mid-Infrared Transmission Microspectroscopy", in *Handbook of Vibrational Spectroscopy*, J. M. Chalmers and P. R. Griffiths, Eds. (Wiley, UK, 2002), p. 1369.
17. S. A. Stewart and A. J. Sommer, *Microsc. Microanal.* **3**, 837 (1997).
18. R. Bhargava, S. Wang, and J. L. Koenig, *Appl. Spectrosc.* **52**, 323 (1998).
19. M. Romeo and M. Diem, *Vib. Spectrosc.* **38**, 129 (2005).
20. M. Romeo and M. Diem, *Vib. Spectrosc.* **38**, 115 (2005).
21. B. Mohlenhoff, M. Romeo, M. Diem, and B. R. Wood, *Biophys. J.* **88**, 3635 (2005).
22. H. J. Gulley-Stahl, A. P. Evan, and A. J. Sommer, "Evanescent Wave Imaging", in *Vibrational Spectroscopic Imaging for Biomedical Applications*, G. Srinivasan, Ed. (McGraw Hill, New York, 2010).
23. B. Goode, "Urology: ATR-FTIR gets to the core of kidney stone development", in *BioOptics World*, May/June (2009).
24. A. J. Sommer, L. G. Tisinger, C. Marcott, and G. M. Story, *Appl. Spectrosc.* **55**, 252 (2001).
25. M. Born and E. Wolf, *Principles of Optics* (Pergamon Press, Oxford, 1965), Third ed.
26. L. Tisinger, Ph.D. Dissertation, Miami University, Oxford, OH (2002).
27. N. J. Harrick, *Phys. Rev. Lett.* **4**, 224 (1960).
28. J. Fahrenfort, *Spectrochimica Acta* **17**, 698 (1961).
29. T. Nakano and S. Kawata, *Bunko Kenkyu* **41**, 377 (1992).
30. T. Nakano and S. Kawata, *Scanning* **16**, 368 (1994).
31. W. J. Smith, *Modern Optical Engineering: The Design of Optical Systems* (McGraw-Hill, New York, 1966).
32. L. L. Lewis and A. J. Sommer, *Appl. Spectrosc.* **53**, 375 (1999).
33. L. L. Lewis and A. J. Sommer, *Appl. Spectrosc.* **54**, 324 (2000).
34. B. M. Patterson and G. J. Havrilla, *Appl. Spectrosc.* **60**, 1256 (2006).
35. "Spatial Resolution in ATR FT-IR Imaging: Measurement and Interpretation" (Technical Note, Perkin Elmer, 2006).
36. H. J. Gulley-Stahl, J. A. Haas, K. A. Schmidt, A. P. Evan, and A. J. Sommer, *Appl. Spectrosc.* **63**, 759 (2009).
37. R. P. Bauman, *Absorption Spectroscopy* (John Wiley and Sons, New York, 1962).
38. E. D. Olsen, *Modern Optical Methods of Analysis* (McGraw Hill, New York, 1975).